



Microstructures and Mechanical Properties of As Cast $(\text{Al}_{7.5}\text{Co}_{21.9}\text{Cr}_{10.9}\text{Ti}_{5.0}\text{Fe}_{21.9}\text{Ni}_{32.8})_{100-x}\text{Cu}_x$ High-Entropy Alloys

Jiajun Li¹, Yu Dong¹, Zemin Wang^{1*}, Min Liu¹, Yi Ding², Bin Fu¹ and Zhanyong Wang^{1*}

¹School of Materials Science and Engineering, Shanghai Institute of Technology, Shanghai, China, ²Baowu Special Metallurgy Co., Ltd., Shanghai, China

OPEN ACCESS

Edited by:

Tao Yang,
City University of Hong Kong, Hong
Kong SAR, China

Reviewed by:

Ji Gu,
Central South University, China
Jinxiong Hou,
City University of Hong Kong, Hong
Kong SAR, China

*Correspondence:

Zemin Wang
wzm@sit.edu.cn
Zhanyong Wang
zhanyong.wang@vip.sina.com

Specialty section:

This article was submitted to
Structural Materials,
a section of the journal
Frontiers in Materials

Received: 29 October 2021

Accepted: 29 November 2021

Published: 21 December 2021

Citation:

Li J, Dong Y, Wang Z, Liu M, Ding Y,
Fu B and Wang Z (2021)
Microstructures and Mechanical
Properties of As Cast
 $(\text{Al}_{7.5}\text{Co}_{21.9}\text{Cr}_{10.9}\text{Ti}_{5.0}\text{Fe}_{21.9}\text{Ni}_{32.8})_{100-x}\text{Cu}_x$ High-Entropy Alloys.
Front. Mater. 8:804918.
doi: 10.3389/fmats.2021.804918

This study focused on the role of Cu in the microstructure characteristics and tensile properties of novel L₁₂-strengthened multicomponent high-entropy alloys (HEAs). A series of as-cast $(\text{Al}_{7.5}\text{Co}_{21.9}\text{Cr}_{10.9}\text{Ti}_{5.0}\text{Fe}_{21.9}\text{Ni}_{32.8})_{100-x}\text{Cu}_x$ ($x = 0.5, 2.5, 5.0$) high-entropy alloys (HEAs) were prepared. The microstructures and mechanical properties of HEAs were investigated using X-ray diffraction, a scanning electron microscope, a transmission electron microscope, and atom probe tomography. The XRD patterns of HEAs confirmed that all HEAs consisted of the FCC phase and the L₁₂ phase. As Cu content increased, the dendritic was gradually coarsened. The spherical L₁₂ size decreased, and number density increased in the interdendritic regions (ID). The L₁₂ mainly contained Ni, Ti, Al, and Cu. The acicular L₁₂ size increased and was continuously distributed in the dendritic regions (DR) as the Cu content increased gradually. The ultimate strength and elongation decreased from 1,002 MPa, 20.0% to 906 MPa, 13.1%, respectively. The segregation rates of Ti, Cu, and Al increased in the DR and ID. The L₁₂ nano-precipitates in the DR become denser and finer, while the L₁₂ islets in the ID region increase and elongate. Large lattice distortion caused by Cu addition weakens the strength of the L₁₂-FCC phase boundary, leading to the premature fracture of the three HEAs, which were the main reasons for the decreases in strength and ductility as Cu content increased.

Keywords: high-entropy alloys, Cu, dendrite, cast, mechanical properties

INTRODUCTION

High-entropy alloys (HEAs) or multi-element alloys, first proposed by Yeh et al. (2004) and Cantor et al. (2004), consist of at least five principal metallic elements. HEAs exhibit huge application potential as structural materials owing to their exceptional mechanical properties. In previous studies, a variety of HEAs have been developed with higher strength, such as dislocation hardening (Fu et al., 2016; Sathiyamoorthi et al., 2019), solid-solution strengthening (Zhou et al., 2007; He et al., 2014), and precipitate microstructures (Tsai et al., 2009; He et al., 2014; Choudhuri et al., 2015; He et al., 2016; Liu et al., 2016; Zhao et al., 2018; Jo et al., 2019). The strength of HEAs can be effectively enhanced by the uniform distribution of nano-sized coherent precipitates, for instance, the L₁₂ and B₂ phases (Wang et al., 2017; Hwang et al., 2020). Recently, Fan et al. (2020) innovatively constructed nano-lamellar architectures in L₁₂-enhanced HEAs. The coherent nano-lamellar strategy, composed

of order-L1₂ and disorder-FCC phases, can markedly improve mechanical properties. Outstanding strength-ductility combination derive from the strong obstacle of the coherent phase boundary to dislocation (Gwalani et al., 2021). L1₂-strengthened HEAs also have many toughening mechanisms, such as coherent nanoparticle-strengthening (Yang et al., 2019), dislocation-induced microbands (Yang et al., 2018), and dynamic refined stacking faults (Tong et al., 2019). Coherent nanophase strengthening in HEAs can obtain a satisfying combination of strength and ductility, equipping HEAs with impressive mechanical properties.

Except for the L1₂ or B₂ phases, the addition of Cu elements also has significant effects on the microstructure and mechanical properties of HEAs. Cu is regarded as an essential element that is widely employed to stabilize nano-precipitates (Gwalani et al., 2017), enhance mechanical properties (Zhang et al., 2017), and improve wear resistance (Verma et al., 2019). It is also considered a stable element of the FCC phase (Tung et al., 2007; Fu et al., 2016; Munitz et al., 2018), and ameliorates the plasticity of HEAs. However, the role of Cu in the microstructure and mechanical properties of Cu-containing HEAs is not clear. For example, a pure Cu phase in interdendritic regions was reported in the Co-Cr-Cu-Fe-Ni system (Verma et al., 2019), and a Cu-rich phase was found in interdendritic regions (Wu et al., 2018). The addition of Cu has also revealed different mechanical properties in different studies (Qin et al., 2019; Yu et al., 2020). Yu et al. (2020) posited that uncontrollable Cu-segregation during the casting process leads to ambiguous phase constitution, which induces conflicting conclusions. Therefore, further study of the role of Cu is crucial to the composition design and performance improvement of high-performance HEAs.

In this study, a series of HEAs with different Cu content were designed by minor additions of Cu. The study encompassed three as-cast HEAs: (Al_{7.5}Co_{21.9}Cr_{10.9}Ti_{5.0}Fe_{21.9}Ni_{32.8})_{99.5}Cu_{0.5} (Cu0.5), (Al_{7.5}Co_{21.9}Cr_{10.9}Ti_{5.0}Fe_{21.9}Ni_{32.8})_{97.5}Cu_{2.5} (Cu2.5), and (Al_{7.5}Co_{21.9}Cr_{10.9}Ti_{5.0}Fe_{21.9}Ni_{32.8})₉₅Cu₅ (Cu5.0) (at. %). The structure, element distribution, phase composition, and mechanical properties of the three as-cast HEAs were systematically studied. The aim was to gain insight into the microstructure and mechanical properties of as-cast HEAs, especially the effects of Cu content on the phase, strength, and plasticity, as well as the composition, morphology, and distribution of the coherent L1₂ phase in an FCC matrix.

MATERIALS AND METHODS

In the present study, a series of HEAs with a nominal composition of (Al_{7.5}Co_{21.9}Cr_{10.9}Ti_{5.0}Fe_{21.9}Ni_{32.8})_{100-x}Cu_x (x = 0.5, 2.5, 5.0 at %) were prepared by the arc melting technique in a high-purity argon atmosphere and cast into a water-cooled copper mold. The alloys were first cooled to 800°C in the mold and then quenched in water. The seven elements constituting the alloy (Al, Co, Cr, Ti, Fe, Ni, and Cu) had a purity greater than 99.95 wt%. The metals were smelted at least five times to ensure chemical homogeneity. Specimens were milled to a size of 6 × 100 × 100 mm³ and were then cut by electrical discharge

machining for microstructure characterization and the tensile test. The crystalline structures of the HEAs were analyzed by X-ray diffraction (XRD, D/Max2500 V) using Cu Kα1 radiation, and the working voltage and current were 30 kV and 20 mA, respectively. The scanning step was 0.02°, and the angular 2θ range was 20° < 2θ < 100°.

The metallographic structures of the HEAs were initially observed by a scanning electron microscope (SEM, Quanta 250 operated at 10 kV) after grinding, mechanical polishing, and etching with ferric chloride solution. Further component analysis and microstructural characterization were conducted using a SEM (Zeiss Gemini 300 operated at 15 kV) equipped with an energy-dispersive X-ray spectroscopy (EDS, AZtec X-MAX) unit and a transmission electron microscope (TEM, Tecnai G2 operated at 200 kV). TEM thin foil specimens were electropolished using a mixture of 93% ethanol and 7% perchloric acid (vol. %) under −35°C. Afterward, the samples were thoroughly cleaned with ethyl alcohol. The related phases of the specimens were characterized by bright-field (BF) TEM imaging, dark-field (DF) TEM imaging, and selected area electron diffraction (SAED) analysis.

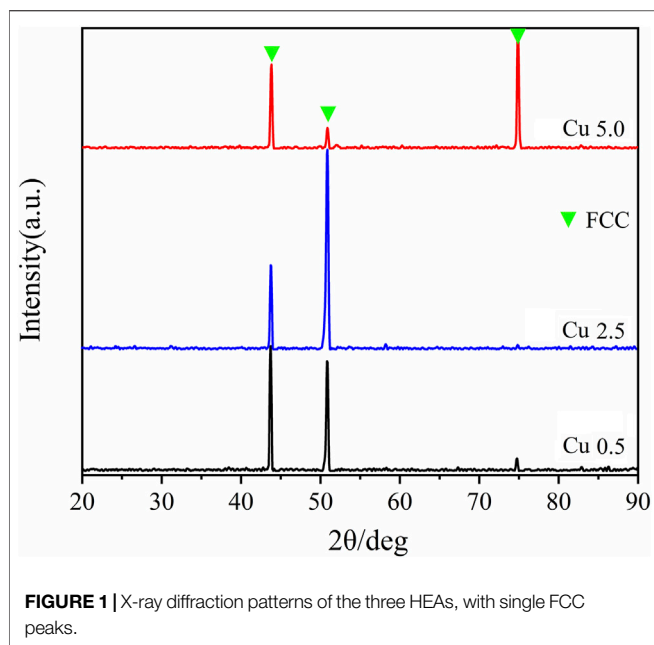
Atom probe tomography (APT) analyses were performed using a CAMECA LEAP 4000X HR atom probe in laser mode at a pulse repetition frequency of 200 kHz. The detection efficiency of the instrument was ~37%. Needle-like specimens used for APT analyses were first cut from bars into rods with cross-sections of 0.5 × 0.5 mm² and then prepared by a two-step electro-polishing procedure (Blum et al., 2016). The reconstruction and quantitative analyses of APT data were performed using Cameca IVAS 3.4.6 software. The L1₂ nano-precipitates were highlighted by 66% Ni+Al+Ti isoconcentration surfaces.

The tensile test was carried out on the Zwick/Roell Z20 universal testing machine at room temperature. The dog-bone-shaped tensile sample had a gauge length of 15 mm, a width of 5 mm, and a thickness of 1.2 mm. The strain rate was 2.0 × 10^{−3} s^{−1}, and a high-resolution strain extensometer was attached to the gauge length section. Fracture surfaces of tensile samples were observed by SEM (FEI-Quanta 250). The crack extension of the HEAs was observed by an optical microscope (OM, Zeiss Axio Observer D1M) after mechanical grinding, polishing, and etching.

RESULTS AND DISCUSSION

XRD Investigation

The XRD patterns of the as-casted Cu 0.5, Cu 2.5, and Cu 5.0 HEAs are shown in **Figure 1**. The Cu 0.5, Cu 2.5, and Cu 5.0 HEAs exhibit similar patterns, but only a typical FCC structure can be detected in all three alloys. However, the diffraction intensity of the three alloys at the same position is not consistent, which is attributed to the preferential orientation of grains during the casting process (Cullity and Stock, 1959). As the Cu content increases, the diffraction peaks gradually shift to the left. The average lattice constants of Cu 0.5, Cu 2.5, and Cu 5.0 HEAs, as measured by XRD, are 3.592, 3.597, and 3.600 Å, respectively.

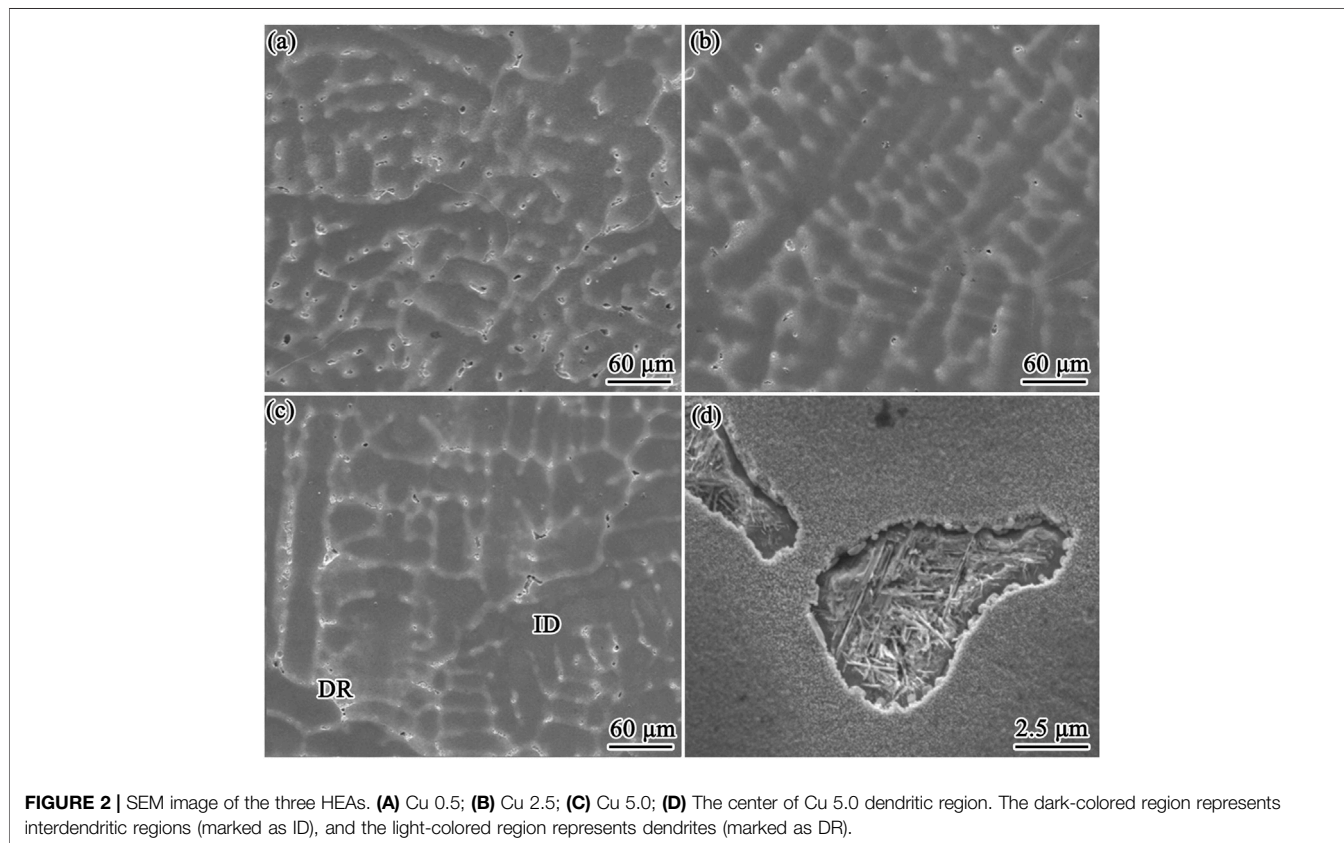


Microstructure and Chemical Analysis

The microstructural evolution of Cu 0.5, Cu 2.5, and Cu 5.0 HEAs is presented in **Figure 2**. All three as-cast HEAs have a typical dendrite (DR, dark) and interdendritic structure (ID, white).

However, the dendritic structure becomes coarser as Cu content increases, and the size of the ID also increases. In general, the size of the dendritic structure is associated with the subcooling of the alloys during the solidification process (Hunt, 1979). As Cu content increases, the solidification temperature decreases, which leads to the decrease of undercooling. Therefore, the velocity of the dendritic structures' growth gradually declines, which coincides with the findings of Wang and Kong (2021) in CoCrFeNiCu_x HEAs.

Moreover, the presence of dendrites leads to the segregation of alloying elements. This was also supported by the numerical modeling of segregation in cast alloys from Nastac (1999). To investigate the element distribution, element mapping was performed in the DR and ID regions of the three HEAs, which is shown in **Figure 3**. The DR and ID region elements for each HEA are summarized in **Table 1**. The segregation degree of each element, expressed by the segregation rates, was calculated by dividing an element's content at the ID by that at the DR region, and is summarized in **Figure 4**. As Cu content increases, Ti, Al, Cu, and Ni are gradually enriched in the DR, while Co, Cr, and Fe are gradually enriched in ID. Meanwhile, the Ni, Ti, and Al content slightly decreases in the DR regions and does not significantly change in the ID (**Table 1**). The ratios of the Ni and Cu atoms to the Ti and Al atoms are close to 3 at the DR regions in the three HEAs, suggesting that the DR microstructures are in the $L1_2$ phase (acicular, **Figure 2D**), with the main content of $(\text{Ni, Cu})_3(\text{Al, Ti})$. The dendrite microstructures become coarser, and the $L1_2$ phase in



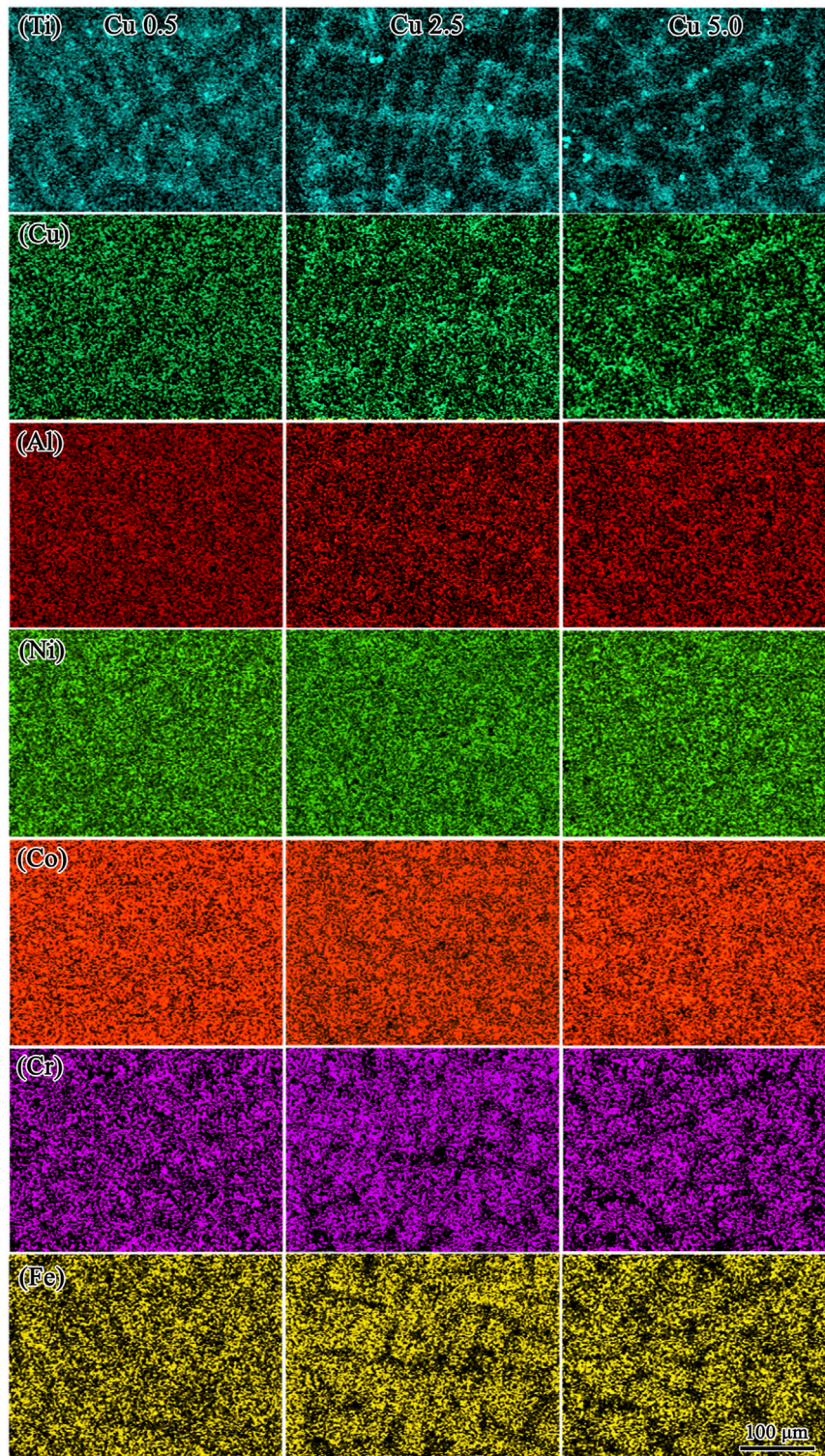


FIGURE 3 | EDS-mapping in the non-etching areas of the three alloys Cu 0.5, Cu 2.5, and Cu 5.0.

the DR region is continuously distributed as the Cu content increases. There is also high atomic radius element (Ti, Al, and Cu) segregation, leading to large lattice distortion between the ID

and DR regions. Lattice distortion can be quantified by the atomic size parameter, δ . The calculation formula of δ (Zhang et al., 2008) is as follows:

TABLE 1 | EDS results (at. %) of the dendrite region and inter-dendrite region of the three HEAs.

Sample	Element	Al	Co	Cr	Ti	Fe	Ni	Cu
Cu 0.5	ID	7.82	21.27	9.58	6.82	18.65	35.06	0.81
	DR	6.61	22.82	12.21	3.19	24.17	30.26	0.76
Cu 2.5	ID	7.72	19.96	8.18	8.36	15.99	34.85	4.95
	DR	6.56	21.54	11.83	3.12	23.16	30.32	3.47
Cu 5.0	ID	8.10	18.44	7.98	8.03	15.78	32.34	9.33
	DR	6.18	22.13	11.73	2.26	23.87	28.50	5.33

$$\delta = \sqrt{\sum_{i=1}^n c_i \left(1 - r_i/\bar{r}\right)^2},$$

where c_i and r_i are the atomic percentage and the atomic radius of the i th component, respectively. It is easy to find that an increase in the content of elements with a large atomic radius will increase the value of δ , indicating greater lattice distortion. These results match those observed in earlier studies, such as $\text{Al}_{0.4}\text{CoCrCuFeNi}$ (Zhou et al., 2020), FeCoNiCuMo_x (molar rates $X = 0.2, 0.4, 0.6, 0.8, 1$) (Soni et al., 2020), and FeCoNiAlCu (Cai et al., 2017).

Figure 5 shows the TEM dark-field (DF) images and the selected area electron diffraction (SAED) of Cu 0.5, Cu 2.5, and Cu 5.0 HEAs at the ID, showing coherent L_{12} spherical nanoscaled precipitates in the FCC matrix. Increasing the Cu concentration promotes the density of L_{12} spherical precipitates. This process is essentially the increase of the L_{12} -FCC coherent interface. **Figure 5D** shows high-resolution TEM (HRTEM) images of the FCC matrix and L_{12} precipitates. A coherent interface with continuous crystal lattices can be observed. The lattice constants of Cu 0.5, Cu 2.5, and Cu 5.0 HEAs are 3.644, 3.661, and 3.676 Å, respectively, which agrees with the XRD results. The lattice mismatches between the two phases are 0.14, 0.16, and 0.19%, respectively. In the study of Xu et al. (2015), coherent nanophase separation could effectively reduce the lattice distortion caused by atomic size difference. Therefore,

it is possible that the addition of Cu increases the lattice distortion and promotes the formation of more L_{12} -FCC coherent interfaces. Moreover, the average size of spherical precipitates is not significantly different between Cu 0.5 and Cu 2.5, but decreases in Cu 5.0. The Cu-rich clusters can act as nucleation sites for the L_{12} precipitates in $\text{Al}_{0.3}\text{CuFeCrNi}_2$ HEA, which leads to a more homogeneous distribution of L_{12} precipitates (Gwalani et al., 2017). Therefore, as Cu content increases, the number density of the Cu-rich clusters increases, which leads the average size of spherical precipitates to decrease, especially in Cu 5.0 HEA.

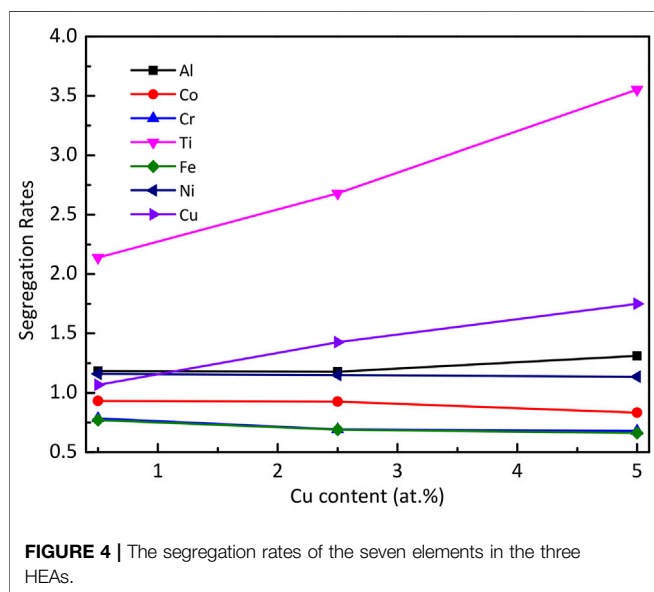
To further investigate the L_{12} phase of the three HEAs, we examined the element distribution and the proxigram of L_{12} (66% Ni+Al+Ti iso-surfaces), which are shown in **Figure 6**. As Cu content increases, the size of spherical L_{12} phase is reduced, but the number density is increased. The content of Fe, Cr, and Co is basically unchanged in the FCC matrix, while the Ti, Al, and Cu content is increased in the L_{12} precipitates. The enrichment of these three large atomic radius elements will increase the local atomic size parameter, δ , of the L_{12} precipitates and hence precipitate more L_{12} coherent nano-precipitates. Fine and numerous coherent nano-precipitates usually contribute to increasing both the tensile strength and ductility of HEAs.

Tensile Properties

Figure 7 depicts the tensile engineering stress-strain curves of the three HEAs at room temperature. The ultimate tensile strengths of Cu 0.5, Cu 2.5, and Cu 5.0 are 1,003, 955, and 904 Mpa, respectively, and the uniform elongations are 20.1, 16.5, and 13.1%, respectively. With the increase of Cu content, the tensile strength and elongation of the sample decrease obviously. Every addition of 2.5 (at. %) Cu lowers the tensile strength of the alloy by about 50 MPa and decreases elongation by about 3.5%. The relationship between tensile strength, elongation, and Cu content is also shown in **Figure 7**. As the Cu content increases, the tensile strength and elongation decrease simultaneously.

The fracture surfaces of the three HEAs are shown in **Figure 8**. The fracture morphology shows that the crack is propagated along the ID/DR boundary. The typical dendrite spacing is selected from the fracture SEM images. The dendrite spacing of Cu 0.5, Cu 2.5, and Cu 5.0 is about 15.5, 29.4, and 39.4 μm , respectively, which also agrees with the microstructures of the three HEAs in **Figure 2**. **Figure 9** shows the crack propagations of the three HEAs observed by OM. The bright and dark regions are the FCC and L_{12} phase, respectively, which corresponds to the DR and ID region in SEM images (**Figure 2**). Combining the SEM images, element mapping, and OM images, the cracks propagate through the L_{12} phase/FCC interfaces during the tensile process. With the increase of Cu content, the dendrite becomes coarser, which may cause a decrease in tensile strength and ductility.

It is noteworthy that the initial part of the tensile stress-strain curves of the three HEAs almost completely coincide. All three HEAs break suddenly at the stage of stress rise. According to previous studies (He et al., 2016; Yang et al., 2020), the increased coherent interface in ID often improves the tensile strength, and the fine dispersion precipitation usually improves the ductility.

**FIGURE 4** | The segregation rates of the seven elements in the three HEAs.

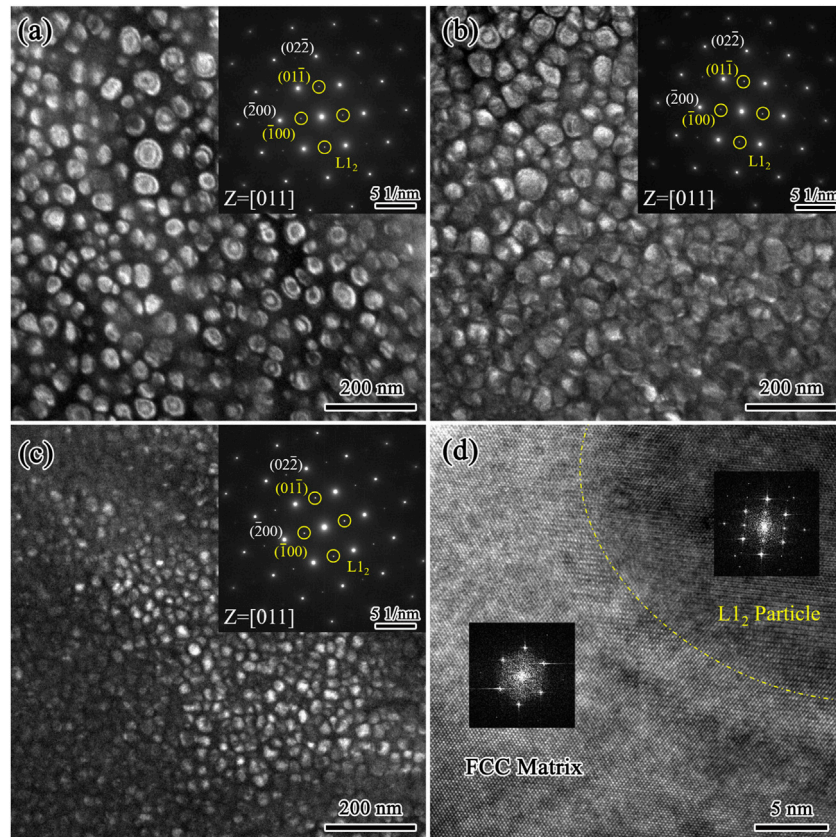


FIGURE 5 | The selected area electron diffraction (SAED) and TEM dark-field (DF) images of **(A)** Cu 0.5; **(B)** Cu 2.5; **(C)** Cu 5.0 HEAs at the interdendritic region. **(D)** HRTEM images of precipitates from the Cu 2.5, and Fourier transformation of the FCC matrix and L_{12} precipitates.

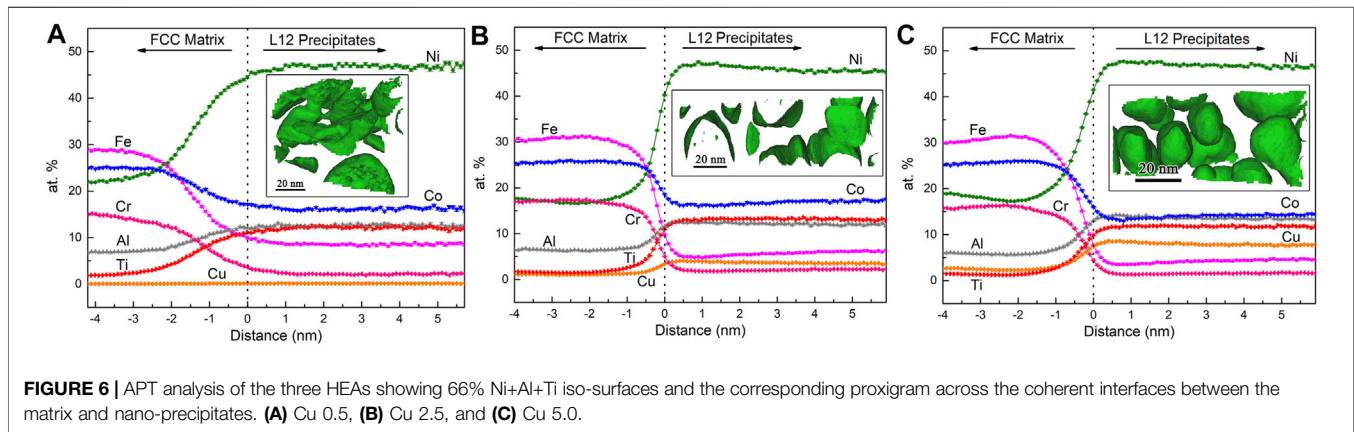


FIGURE 6 | APT analysis of the three HEAs showing 66% Ni+Al+Ti iso-surfaces and the corresponding proxigram across the coherent interfaces between the matrix and nano-precipitates. **(A)** Cu 0.5, **(B)** Cu 2.5, and **(C)** Cu 5.0.

Therefore, the observed decrease in tensile strength and elongation indicates that the fracture is most likely to originate from the DR region rather than the ID. Among the three HEAs in this study, Ti, Al, and Cu segregate violently at the DR region. Severe segregation will decrease the ductility of alloys (Yu et al., 2020). The segregation of Ti, Al, and Cu will also lead to a large lattice mismatch at the coherent interface, making these DR regions harmful to tensile strength.

To further explain the ductility and strength decrease mechanism of the three HEAs with increasing Cu content, a schematic diagram was set up, as shown in **Figure 10**. In the Cu 0.5 HEA, the FCC/ L_{12} interfacial bonding strength is strong, the DR region is not continuous as shown in **Figure 10A**, and the fracture passes through the ID region inevitably. As Cu content increases, the increase of segregation leads to a serious lattice mismatch and a decrease of interfacial bonding strength. More

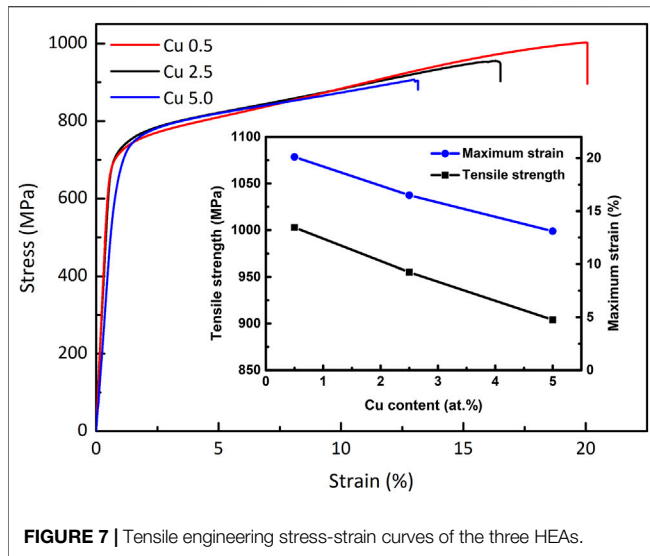


FIGURE 7 | Tensile engineering stress-strain curves of the three HEAs.

$L1_2$ makes the DR region extend and connect, and the ID region where the fracture passes through becomes shorter in the Cu 2.5 HEA (**Figure 10B**). Finally, in the Cu 5.0 HEA, the fracture propagates directly along the continuously DR region (**Figure 10C**), and the tensile strength and ductility of the alloy are further reduced. This decrease of mechanical properties is due to the breakable microstructure of as-cast HEAs. The HEAs fracture through the DR region in advance when the potential of the ID has not been fully exploited. In contrast, the microstructure of HEAs in some studies (Gwalani et al., 2017) has been relatively fine and uniform, and the ductility and tensile properties of HEAs in these studies have increased with increasing Cu content. Moreover, in other studies (Qin et al., 2019; Yu et al., 2020), the addition of Cu has led to the phase evolution of HEAs, and the mechanical properties of HEAs have been diverse owing to the different phase compositions. Cu has had different modes of effects on HEAs in such studies, so different conclusions have been drawn.

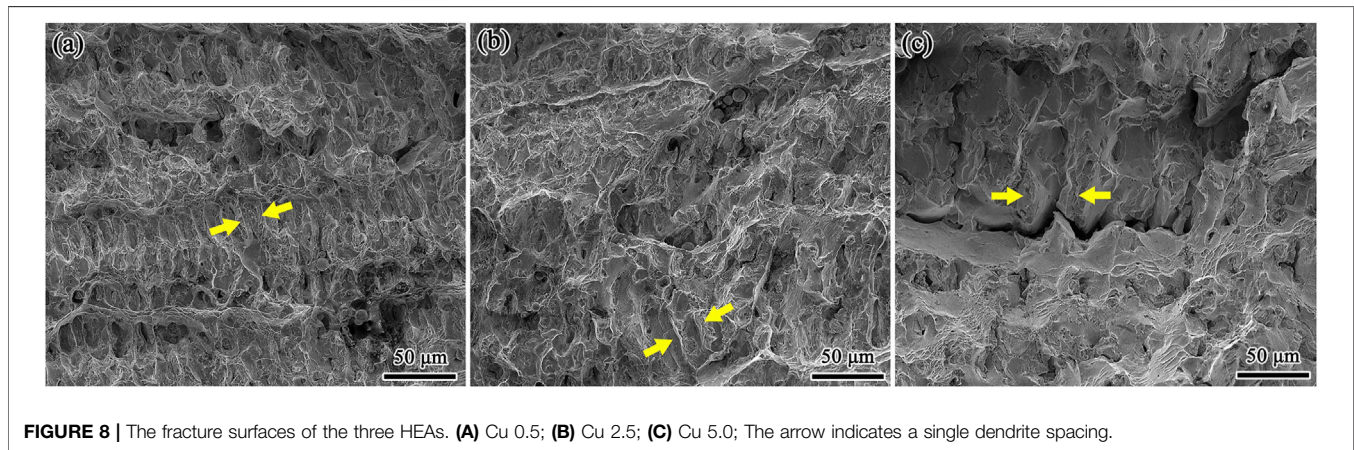


FIGURE 8 | The fracture surfaces of the three HEAs. (A) Cu 0.5; (B) Cu 2.5; (C) Cu 5.0; The arrow indicates a single dendrite spacing.

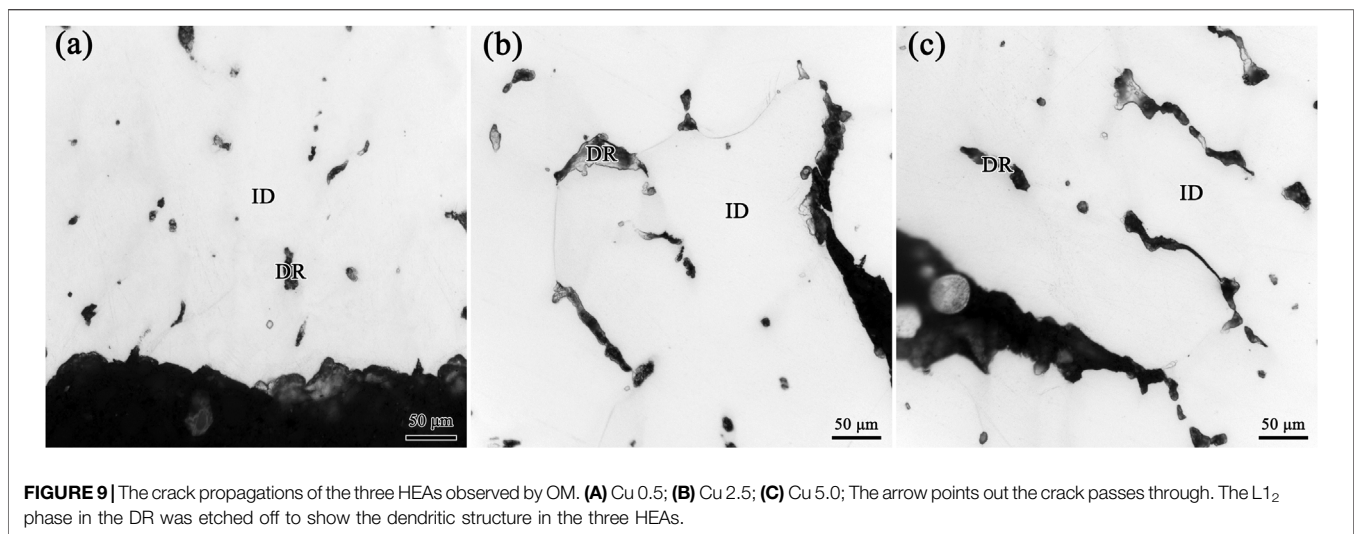
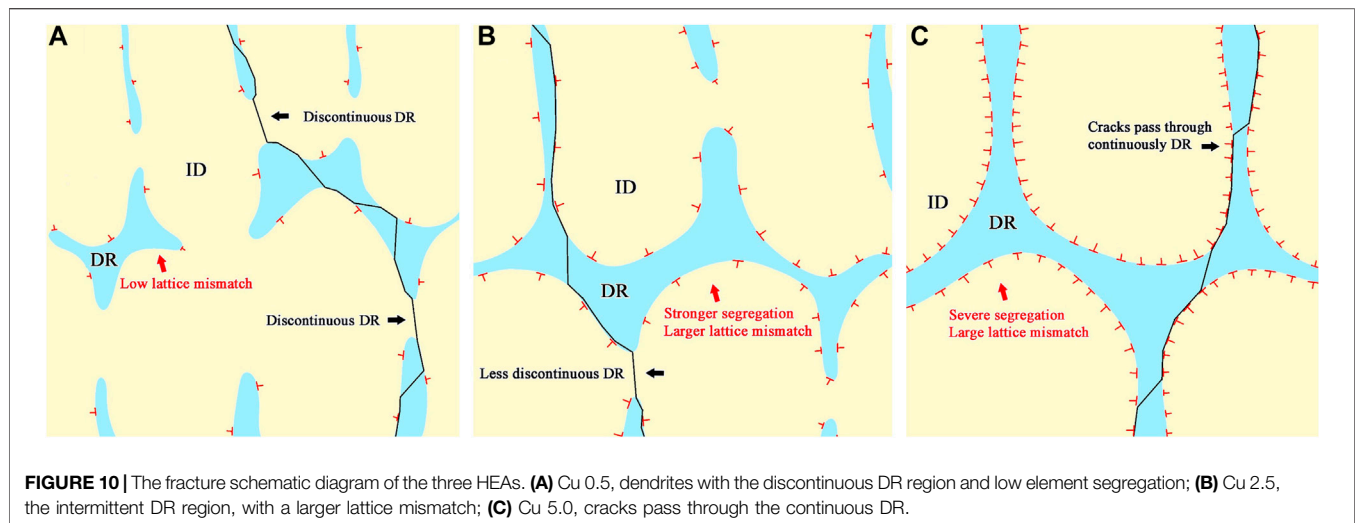


FIGURE 9 | The crack propagations of the three HEAs observed by OM. (A) Cu 0.5; (B) Cu 2.5; (C) Cu 5.0; The arrow points out the crack passes through. The $L1_2$ phase in the DR was etched off to show the dendritic structure in the three HEAs.



CONCLUSION

The present study mainly focused on the effect of Cu content in the microstructures and mechanical properties of as-cast high-entropy alloys. The following conclusion were drawn:

- 1) With the increase of Cu content, the dendritic structure of as-cast HEAs gradually coarsens. The typical dendrite spacing of Cu 0.5, Cu 2.5, and Cu 5.0 is about 15.5, 29.4, and 39.4 μm , respectively.
- 2) Cu is beneficial to promote the segregation of elements with a large atomic radius, such as Ti and Al, which will lead to aggravated lattice distortion. The $L1_2$ nano-precipitates in the ID become denser and finer, while the $L1_2$ islets in the DR region increase and elongate.
- 3) Large lattice distortion caused by Cu addition weakens the strength of the $L1_2$ -FCC phase boundary in the DR region, leading to the premature fracture of the three HEAs.
- 4) The large lattice distortion and stress of the coarsened dendrite are the main reasons for the decreases in strength and ductility.

DATA AVAILABILITY STATEMENT

The original contributions presented in the study are included in the article/Supplementary Material, further inquiries can be directed to the corresponding authors.

REFERENCES

- Blum, I., Cuvilly, F., and Lefebvre-Ulrikson, W. (2016). "Atom Probe Sample Preparation," in "Chapter Four - Atom Probe Sample Preparation" in *Atom Probe Tomography Put Theory into Practice*. Editors W.L. Ulrikson, F. Vurpillot, and X. Sauvage (Salt Lake City, Utah: Academic Press), 97–121. doi:10.1016/b978-0-12-804647-0.00004-8
- Cai, Z., Wang, Y., Cui, X., Jin, G., Li, Y., Liu, Z., et al. (2017). Design and Microstructure Characterization of FeCoNiAlCu High-Entropy alloy Coating by Plasma Cladding: In Comparison with Thermodynamic Calculation. *Surf. Coat. Tech.* 330, 163–169. doi:10.1016/j.surfcoat.2017.09.083
- Cantor, B., Chang, I. T. H., Knight, P., and Vincent, A. J. B. (2004). Microstructural Development in Equiatomic Multicomponent Alloys. *Mater. Sci. Eng. A* 375–377, 213–218. doi:10.1016/j.msea.2003.10.257
- Choudhuri, D., Alam, T., Borkar, T., Gwalani, B., Mantri, A. S., Srinivasan, S. G., et al. (2015). Formation of a Huesler-like L21 Phase in a CoCrCuFeNiAlTi High-Entropy alloy. *Scripta Materialia* 100, 36–39. doi:10.1016/j.scriptamat.2014.12.006
- Cullity, B. D., and Stock, S. R. (1959). *Elements of X-ray Diffraction*. New Jersey: Addison-Wesley Publishing Co., 514p.

AUTHOR CONTRIBUTIONS

JL performed all the experiments, analyzed the experimental results as part of his Master Degree research, made a first draft, with substantial input, writing efforts, and discussions from YuD, ML, YiD, BF, and ZW. ZW provided general concept of this study, support, and supervision of experiments.

FUNDING

This work was supported by the Natural Science Foundation of China (No. 51874198), Shanghai Sailing Program (NO 19YF1446600), Project of the State Key Laboratory for Advanced Metals and Materials of PR China (2018-Z05) and Shanghai Science and Technology Committee of PR China (16090503600, 19YF1446600).

ACKNOWLEDGMENTS

The authors acknowledge the contribution of Liu Renduo from Shanghai Institute of Applied Physics, Chinese Academy of Sciences, who performed TEM/SAED analyses of the HEAs, and Dr. Li Hui from Shanghai University who performed APT analyses of the HEAs. The authors also thank Shiyanjia Lab (www.shiyanjia.com) for the EDS measurement.

- Fan, L., Yang, T., Luan, J. H., and Jiao, Z. B. (2020). Control of Discontinuous and Continuous Precipitation of γ' -strengthened High-Entropy Alloys through Nanoscale Nb Segregation and Partitioning. *J. Alloys Compd.* 832, 154903. doi:10.1016/j.jallcom.2020.154903
- Fu, Z., Chen, W., Wen, H., Zhang, D., Chen, Z., Zheng, B., et al. (2016). Microstructure and Strengthening Mechanisms in an FCC Structured Single-phase Nanocrystalline Co₂₅Ni₂₅Fe₂₅Al_{7.5}Cu_{17.5} High-Entropy alloy. *Acta Materialia* 107, 59–71. doi:10.1016/j.actamat.2016.01.050
- Gwalani, B., Choudhuri, D., Soni, V., Ren, Y., Styles, M., Hwang, J. Y., et al. (2017). Cu Assisted Stabilization and Nucleation of L12 Precipitates in Al_{0.3}CuFeCrNi₂ Fcc-Based High Entropy alloy. *Acta Materialia* 129, 170–182. doi:10.1016/j.actamat.2017.02.053
- Gwalani, B., Dasari, S., Sharma, A., Soni, V., Shukla, S., Jagetia, A., et al. (2021). High Density of strong yet Deformable Intermetallic Nanorods Leads to an Excellent Room Temperature Strength-Ductility Combination in a High Entropy alloy. *Acta Materialia* 219, 117234. doi:10.1016/j.actamat.2021.117234
- He, J. Y., Liu, W. H., Wang, H., Wu, Y., Liu, X. J., Nieh, T. G., et al. (2014). Effects of Al Addition on Structural Evolution and Tensile Properties of the FeCoNiCrMn High-Entropy alloy System. *Acta Materialia* 62, 105–113. doi:10.1016/j.actamat.2013.09.037
- He, J. Y., Wang, H., Huang, H. L., Xu, X. D., Chen, M. W., Wu, Y., et al. (2016). A Precipitation-Hardened High-Entropy alloy with Outstanding Tensile Properties. *Acta Materialia* 102, 187–196. doi:10.1016/j.actamat.2015.08.076
- Hunt, J. D. (1979). *Solidification and Casting of Metals: Proceedings of an International Conference on Solidification*. London: Metals Society Press.
- Hwang, J. H., Trang, T. T. T., Lee, O., Park, G., Zargarani, A., and Kim, N. J. (2020). Improvement of Strength - Ductility Balance of B2-Strengthened Lightweight Steel. *Acta Materialia* 191, 1–12. doi:10.1016/j.actamat.2020.03.022
- Jo, Y. H., Choi, W. M., Kim, D. G., Zargarani, A., Lee, K., Sung, H., et al. (2019). Utilization of Brittle σ Phase for Strengthening and Strain Hardening in Ductile VCrFeNi High-Entropy alloy. *Mater. Sci. Eng. A* 743, 665–674. doi:10.1016/j.msea.2018.11.136
- Liu, W. H., Lu, Z. P., He, J. Y., Luan, J. H., Wang, Z. J., Liu, B., et al. (2016). Ductile CoCrFeNiCu High Entropy Alloys Strengthened by Hard Intermetallic Phases. *Acta Materialia* 116, 332–342. doi:10.1016/j.actamat.2016.06.063
- Munitz, A., Kaufman, M. J., Nahmany, M., Derimow, N., and Abbaschian, R. (2018). Microstructure and Mechanical Properties of Heat Treated Al_{1.25}CoCrCuFeNi High Entropy Alloys. *Mater. Sci. Eng. A* 714, 146–159. doi:10.1016/j.msea.2017.12.084
- Nastac, L. (1999). Numerical Modeling of Solidification Morphologies and Segregation Patterns in Cast Dendritic Alloys. *Acta Materialia* 47 (17), 4253–4262. doi:10.1016/S1359-6454(99)00325-0
- Qin, G., Zhang, Y., Chen, R., Zheng, H., Wang, L., Su, Y., et al. (2019). Microstructures and Mechanical Properties of (AlCoCrFeMn)_{100-x}Cu_x High-Entropy Alloys. *Mater. Sci. Tech.* 35 (12), 1457–1463. doi:10.1080/02670836.2019.1629541
- Sathiyamoorthi, P., Moon, J., Bae, J. W., Asghari-Rad, P., and Kim, H. S. (2019). Superior Cryogenic Tensile Properties of Ultrafine-Grained CoCrNi Medium-Entropy alloy Produced by High-Pressure Torsion and Annealing. *Scripta Materialia* 163, 152–156. doi:10.1016/j.scriptamat.2019.01.016
- Soni, V. K., Sanyal, S., and Sinha, S. K. (2020). Phase Evolution and Mechanical Properties of Novel FeCoNiCuMox High Entropy Alloys. *Vacuum* 174, 109173. doi:10.1016/j.vacuum.2020.109173
- Tong, Y., Chen, D., Han, B., Wang, J., Feng, R., Yang, T., et al. (2019). Outstanding Tensile Properties of a Precipitation-Strengthened FeCoNiCrTi_{0.2} High-Entropy alloy at Room and Cryogenic Temperatures. *Acta Materialia* 165, 228–240. doi:10.1016/j.actamat.2018.11.049
- Tsai, C.-W., Chen, Y.-L., Tsai, M.-H., Yeh, J.-W., Shun, T.-T., and Chen, S.-K. (2009). Deformation and Annealing Behaviors of High-Entropy alloy Al_{0.5}CoCrCuFeNi. *J. Alloys Compd.* 486, 427–435. doi:10.1016/j.jallcom.2009.06.182
- Tung, C.-C., Yeh, J.-W., Shun, T.-t., Chen, S.-K., Huang, Y.-S., and Chen, H.-C. (2007). On the Elemental Effect of AlCoCrCuFeNi High-Entropy alloy System. *Mater. Lett.* 61 (1), 1–5. doi:10.1016/j.matlet.2006.03.140
- Verma, A., Tarate, P., Abhyankar, A. C., Mohape, M. R., Gowtam, D. S., Deshmukh, V. P., et al. (2019). High Temperature Wear in CoCrFeNiCu High Entropy Alloys: The Role of Cu. *Scripta Materialia* 161, 28–31. doi:10.1016/j.scriptamat.2018.10.007
- Wang, W. L., and Kong, Z. H. (2021). Phase Separation and Microhardness of Rapidly Solidified High-Entropy CoCrFeNiCu Alloys. *J. Alloys Compd.* 853, 156451. doi:10.1016/j.jallcom.2020.156451
- Wang, Z. G., Zhou, W., Fu, L. M., Wang, J. F., Luo, R. C., Han, X. C., et al. (2017). Effect of Coherent L12 Nanoprecipitates on the Tensile Behavior of a Fcc-Based High-Entropy alloy. *Mater. Sci. Eng. A* 696, 503–510. doi:10.1016/j.msea.2017.04.111
- Wu, B., Xie, Z., Huang, J., Lin, J., Yang, Y., Jiang, L., et al. (2018). Microstructures and Thermodynamic Properties of High-Entropy Alloys CoCrCuFeNi. *Intermetallics* 93, 40–46. doi:10.1016/j.intermet.2017.10.018
- Xu, X. D., Liu, P., Guo, S., Hirata, A., Fujita, T., Nieh, T. G., et al. (2015). Nanoscale Phase Separation in a Fcc-Based CoCrCuFeNiAl_{0.5} High-Entropy alloy. *Acta Materialia* 84, 145–152. doi:10.1016/j.actamat.2014.10.033
- Yang, T., Zhao, Y. L., Luan, J. H., Han, B., Wei, J., Kai, J. J., et al. (2019). Nanoparticles-strengthened High-Entropy Alloys for Cryogenic Applications Showing an Exceptional Strength-Ductility Synergy. *Scripta Materialia* 164, 30–35. doi:10.1016/j.scriptamat.2019.01.034
- Yang, T., Zhao, Y. L., Tong, Y., Jiao, Z. B., WeiCai, J. J. X., Cai, J. X., et al. (2018). Multicomponent Intermetallic Nanoparticles and Superb Mechanical Behaviors of Complex Alloys. *Science* 362 (6417), 933–937. doi:10.1126/science.aas8815
- Yang, T., Zhao, Y. L., Fan, L., Wei, J., Luan, J. H., Liu, W. H., et al. (2020). Control of Nanoscale Precipitation and Elimination of Intermediate-Temperature Embrittlement in Multicomponent High-Entropy Alloys. *Acta Materialia* 189 (47), 59–937. doi:10.1016/j.actamat.2020.02.059
- Yeh, J.-W., Chen, S.-K., Lin, S.-J., Gan, J.-Y., Chin, T.-S., Shun, T.-T., et al. (2004). Nanostructured High-Entropy Alloys with Multiple Principal Elements: Novel Alloy Design Concepts and Outcomes. *Adv. Eng. Mater.* 6, 299–303. doi:10.1002/adem.200300567
- Yu, Q., Xu, W.-W., Cui, C., Gong, X., Li, W., Chen, L., et al. (2020). Unveiling Segregation-Induced Evolution in Phase Constitution of Cu-Containing High-Entropy Alloys. *J. Alloys Compd.* 843, 156109. doi:10.1016/j.jallcom.2020.156109
- Zhang, Q., Xu, H., Tan, X. H., Hou, X. L., Wu, S. W., Tan, G. S., et al. (2017). The Effects of Phase Constitution on Magnetic and Mechanical Properties of FeCoNi(CuAl) (X = 0-1.2) High-Entropy Alloys. *J. Alloys Compd.* 693, 1061–1067. doi:10.1016/j.jallcom.2016.09.271
- Zhang, Y., Zhou, Y. J., Lin, J. P., Chen, G. L., and Liaw, P. K. (2008). Solid-Solution Phase Formation Rules for Multi-Component Alloys. *Adv. Eng. Mater.* 10, 534–538. doi:10.1002/adem.200700240
- Zhao, Y. L., Yang, T., Zhu, J. H., Chen, D., Yang, Y., Hu, A., et al. (2018). Development of High-Strength Co-free High-Entropy Alloys Hardened by Nanosized Precipitates. *Scripta Materialia* 148, 51–55. doi:10.1016/j.scriptamat.2018.01.028
- Zhou, E., Qiao, D., Yang, Y., Xu, D., Lu, Y., Wang, J., et al. (2020). A Novel Cu-Bearing High-Entropy alloy with Significant Antibacterial Behavior against Corrosive marine Biofilms. *J. Mater. Sci. Tech.* 46, 201–210. doi:10.1016/j.jmst.2020.01.039
- Zhou, Y. J., Zhang, Y., Wang, Y. L., and Chen, G. L. (2007). Solid Solution Alloys of AlCoCrFeNiTiX with Excellent Room-Temperature Mechanical Properties. *Appl. Phys. Lett.* 90, 181904. doi:10.1063/1.2734517

Conflict of Interest: Author DY is employed by Baowu Special metallurgy Co.,Ltd.

The remaining authors declare that the research was conducted in the absence of any commercial or financial relationships that could be construed as a potential conflict of interest.

Publisher's Note: All claims expressed in this article are solely those of the authors and do not necessarily represent those of their affiliated organizations, or those of the publisher, the editors and the reviewers. Any product that may be evaluated in this article, or claim that may be made by its manufacturer, is not guaranteed or endorsed by the publisher.

Copyright © 2021 Li, Dong, Wang, Liu, Ding, Fu and Wang. This is an open-access article distributed under the terms of the Creative Commons Attribution License (CC BY). The use, distribution or reproduction in other forums is permitted, provided the original author(s) and the copyright owner(s) are credited and that the original publication in this journal is cited, in accordance with accepted academic practice. No use, distribution or reproduction is permitted which does not comply with these terms.